The effect of temperature on lost circulation through induced fractures - a fully coupled THM model

Shuai Zhang
China University of Petroleum-Beijing, Beijing, China

Yongcun Feng
China University of Petroleum-Beijing, Beijing, China

Tao Xie
Tianjin Branch, CNOOC (China) Co., Ltd., Tianjin, China

Qi He
China University of Petroleum-Beijing, Beijing, China

Hai Lin
Tianjin Branch, CNOOC (China) Co., Ltd., Tianjin, China

ABSTRACT: The exploitation of deep oil and gas resources has attracted increased attention. When drilling, a high frequency of lost circulation results from the features of high temperature, high pressure, and high stress, where the temperature is an important factor that cannot be disregarded. The effect of temperature on drilling fluid loss law as well as the influence of temperature difference on fracture initiation, fracture geometry, and fracture extension rate is investigated using a fully coupled Thermal-Hydrological-Mechanical (THM) model built using the finite element method. The simulation results demonstrate that the temperature effect can dramatically lower the lost flow rate. Only when the flow rate is low does temperature dominate the lost fracture extension, which is then divided into the flow-rate dominance stage and temperature dominance stage under high flow rates.

Keywords: Lost Circulation, THM, Fracture Propagation, Dynamic Circulation, Finite element method.

1 INTRODUCTION

Deep oil and gas resources are characterized by high temperature, high pressure, and high stress, which commonly results in lost circulation incidents while drilling and severely impedes the progress of exploration and development. The optimization of plugging materials and the selection of the plugging method are both heavily influenced by lost fracture size. Currently, scholars use analytical solutions and numerical simulations to predict the lost fracture size.

The analytical solution of lost fracture is mainly based on the theory related to hydraulic fracturing. In 2004, Alberty proposed a linear fracture resolution model to determine the size of a single lost fracture in the classic "Stress Cage" study(Alberty & McLean, 2004). Since then, researchers have increasingly taken into account the analytical model of lost fracture size based on it, which is affected by well slope, stress anisotropy, non-uniform intra-seam pressure distribution, and multiple fractures(Y. Feng & K. E. Gray, 2016; Morita & Fuh, 2012; Shahri et al., 2015; van Oort & Razavi, 2014; Zhang et al., 2016). These models, however, are based on the theory of linear elasticity, and the majority of them disregard the impacts of heat transport.

Numerous authors have used numerical simulation techniques to get fracture size prediction findings that are more accurate. Wang investigated the effect of stress concentration around the well on fracture sizes but did not take seepage and heat transfer into account while developing a loss fracture model utilizing boundary element and finite element techniques based on the linear elasticity assumption, respectively(Wang et al., 2009). Feng proposed a loss fracture finite element model based on the pore elasticity hypothesis(Feng et al., 2015; Y. Feng & K. Gray, 2016). Salehi used the cohesive element method, which is frequently used in hydraulic fracturing studies, to simulate the expansion of the lost fracture to investigate the dynamic lost fracture size, but the model directly applied the constant injection rate boundary conditions, which did not correspond to the actual situation(Salehi, 2012). Based on the ABAQUS finite element platform, Feng developed an integrated wellbore circulation-fracture expansion-rock deformation prediction model(Feng & Gray, 2018). However, it has not been reported how heat transfer between the wellbore and the formation affects the propagation of the lost fracture.

In this paper, a fully coupled heat-flow-solid model of dynamic drilling circulation is proposed to simulate dynamic bottom-hole pressure and lost fractures during drilling while taking into account the impact of temperature.

2 ESTABLISHMENT OF THE THM MODEL

2.1 Model Overview

The calculation prototype in this paper is a high-temperature, high-pressure formation in the South China Sea. The formation is 4,500 meters deep, the temperature is 205°C, and the pressure coefficient is 2.04. The geometric model is displayed in Figure 1.

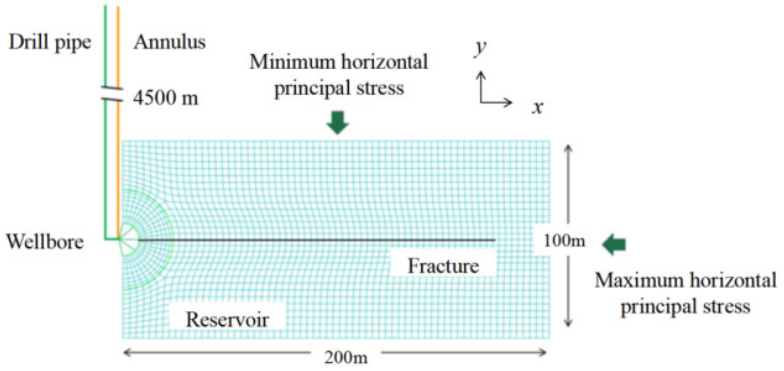

Figure 1. Schematic diagram of drilling fluid lost circulation model.

2.2 Basic Theory

2.2.1 Pipe element flow equation

Based on Bernoulli's equation and the assumption that the fluid is incompressible and a single phase, the viscosity, gravity, and pressure losses of the fluid in the tube are computed. The following describes the flow equation between two nodes in an element (Manual, 2020).

$$\Delta P - \rho_p g \Delta Z = (C_L + K_i)\frac{\rho_p V_p^{\,2}}{2} \tag{1}$$

Where ΔP is the pressure difference between two nodes, ΔZ is the difference in altitude between two nodes, ρ_p is the density of the fluid in the pipe, g is gravity acceleration, C_L is loss coefficient, K_i is directional loss coefficient, V_p is the fluid flow rate in the pipe.

2.2.2 Formation matrix control equation

The constitutive equation of the rock considering thermal porosity elasticity is (Wardeh & Perrin, 2008).

$$\sigma_{ij} = 2G\varepsilon_{ij} + \delta_{ij}(\lambda\varepsilon_{kk} - \frac{E\gamma\Delta T}{1\text{-}2v} + \alpha p) \tag{2}$$

Where G , λ are Lamé constant.

$$G = \frac{E}{2(1+v)}, \lambda = \frac{vE}{(1+v)(1-2v)} \tag{3}$$

Where σ_{ij} is total stress tensor, ε_{ij} is strain tensor, γ is the thermal expansion coefficient of rock, ΔT is temperature variation value of rock, E is Young's modulus of rock, v is Poisson's ratio of rock.

2.2.3 Fracture zone control equation

The traction-separation law is used as the fracture initiation criterion in this paper, and the Cohesive element is used to characterize fracture initiation and extension. If a fracture has opened or not is determined using the quadratic stress criterion (Chen et al., 2010).

The following is the equation for fluid seepage between the fracture surface and formation (Peirce & Detournay, 2008).

$$-\frac{\partial w}{\partial t} + \nabla \cdot q + (q_t + q_b) = 0 \tag{4}$$

Where q is tangential flow fluid flux in the fracture, w is fracture width, q_t and q_b are the normal leak-off velocities at the top and bottom of the fracture, respectively.

The energy balance equation considers the temperature effect within the fracture as follow (Manual, 2020).

$$\begin{aligned} &\rho_f c_f (d\theta)_{,t} + \rho_f c_f \nabla \cdot (d\mathrm{q}\theta) - \nabla \cdot (dk\nabla\theta) - \rho_f c_f \left[c_t(p_i - p_t) + c_b(p_i - p_b)\right] \\ &-h(\theta - \theta_t) - h(\theta - \theta_b) = 0 \end{aligned} \tag{5}$$

Where ρ_f is fluid density in the fracture, c_f is the specific heat capacity of fluid in the fracture, k is the heat transfer coefficient of fluid in the fracture, h is convection heat transfer coefficient, θ is the fluid temperature inside the fracture, θ_t and θ_b are the temperature of the top and bottom surface of the fracture, respectively.

2.3 Input parameters

The model input parameters are shown in Table 1. To characterize the 1/2 formation model with constant displacement, pore pressure, and temperature in the far field, the symmetric boundary condition is applied on the left side, while displacement boundary, pore pressure boundary, and temperature boundary conditions are applied on the other sides.

Table 1. Input parameters of the model.

	Input Parameter	Value	Input Parameter	Value
Rock matrix	Young's modulus (GPa)	27.2	Thermal conductivity (W/(m.℃))	2.596
	Poisson's ratio	0.22	Thermal expansion (10^{-6}/℃)	12.97
	Permeability (mD)	8.4	Temperature (℃)	205
	Specific heat (J/(kg.℃))	878	Porosity ratio	0.2
Cohesive element	Tensile strength (MPa)	5.2	Leak off coefficient (m^2/(Pa.s))	1×10^{-10}
	Fracture energy (N/m)	1000		

3 RESULTS AND DISCUSSIONS

3.1 Temperature field distribution

At a flow rate of 54 m^3/h and a drilling fluid temperature of 25°C, lost circulation occurred. Figure 2 shows the distribution of fracture and temperature field after the occurrence of lost circulation for 24 hours. The temperature in the far field is unaffected, while the temperature variation is present close to the fracture zone. The fracture has a total length of 168.9m and a maximum width of 16.74mm. The front of the temperature field is the same as the front of the fracture, however, the maximum influence width is 6.18m, as shown in Figure 3. During field construction, lost circulation will typically be restored rapidly, with loss timeframes ranging from a few minutes to a few hours. As a result, at this time scale, the circulation of low-temperature drilling fluid will significantly change the temperature field inside the fracture and close to the fracture zone. If the lost time is long enough, the influence range of the temperature field will expand.

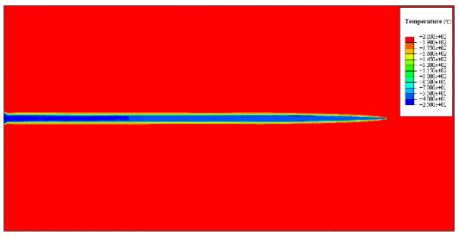

Figure 2. Temperature field distribution.

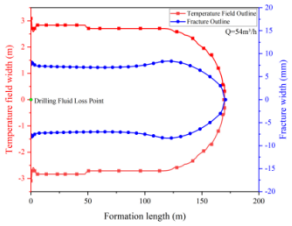

Figure 3. Temperature field and fracture outline.

3.2 Effect of temperature on lost circulation flow rate threshold

A 2.8-meter-long fracture formed at a drilling fluid temperature of 25°C, despite a circulation flow rate of 3.6 m^3/h (Figure 4). The length of the fracture increased with higher flow rates, with a nearly linear increase observed for flow rates below 39.6 m^3/h. However, for flow rates greater than 39.6 m^3/h, the fracture growth process was divided into two stages. In the first stage, the fracture length increased rapidly in a short period, followed by a dramatic slowdown in growth rate in the second stage, which was similar to flow rates below 39.6 m^3/h. Figure 5 demonstrated that, under isothermal conditions, all fractures reached their maximum length quickly, and at a flow rate of 46.8 m^3/h, no fractures were induced. This phenomenon indicates that the bottom hole pressure exceeds the formation fracture pressure when the flow rate exceeds 39.6 m^3/h. Fractures were created at the start of circulation, leading to a rapid increase in fracture length during the first stage, independent of the drilling fluid's temperature. In the second stage, fracture length increased during low-temperature circulation but remained constant during isothermal circulation. Therefore, lost circulation was primarily caused by the flow rate during the initial stage, while the fracture area was stabilized during isothermal circulation. However, non-isothermal circulation caused the formation to shrink due to heat exchange with the low-temperature drilling fluid, leading to further expansion of the fracture length.

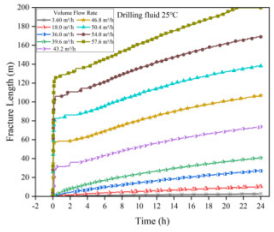

Figure 4. Fracture length vs different flow rates (25 °C).

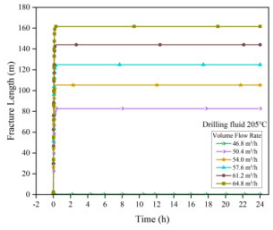

Figure 5. Fracture length vs different flow rates (205 °C).

3.3 Effect of temperature on the size of induced fractures

The lost fracture profiles at isothermal and 25°C conditions are shown in Figures 6 and 7, respectively. In both isothermal and low-temperature circulation, the lost fracture keeps growing as the flow rate goes up. The fracture profile during isothermal cycling is elliptical. In contrast, during 25°C drilling fluid circulation, not only is the fracture longer with the same flow rate, but the average fracture width increased by about 50%, exhibiting a rectangular form.

A simulation of drilling fluid with a temperature range of 25°C to 205°C (with a 50°C interval) and a flow rate of 54m^3/h was performed to further study the impact of temperature difference on the fracture profile. Figures 8 and 9 show the fracture profiles and lengths. There is a noticeable rise in fracture length and width with increasing temperature difference, and it can be seen that the fracture profile at 205°C is elliptical while others are more rectangular. The fracture length increased from 104.5m to 169.2m, a rise of 61.9% when compared to 205°C and 25°C. The greatest fracture width rose by 183.8%, from 5.81mm to 16.43mm. In conclusion, temperature has a considerable impact on fracture size, and this impact increases with increasing temperature differences.

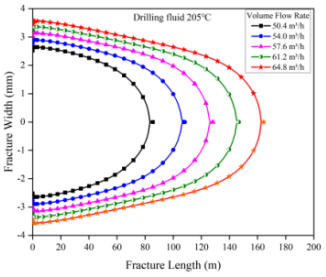

Figure 6. Fracture profile with different flow rates (205 °C).

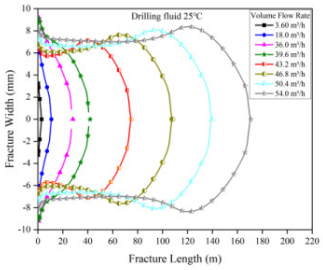

Figure 7. Fracture profile with different flow rates (25 °C).

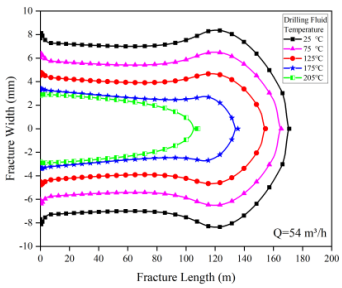

Figure 8. Fracture profile with different temperature differences.

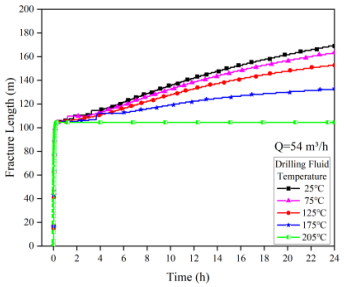

Figure 9. Fracture length with different temperature difference.

4 CONCLUSION

This paper utilizes the finite element method to create a fully coupled THM model for dynamic lost circulation of drilling fluid under ideal formation conditions. The simulation reveals the following findings:

(1) Low-temperature drilling fluid circulation alters the formation's stress and temperature fields, with the temperature field being impacted near the fracture region. A cooling effect occurs when the drilling fluid temperature is lower than that of the formation, resulting in formation contraction and thermal stress-induced fracture, and lost channel development even at a small circulation flow rate.

(2) As the flow rate increases, a two-stage lost fracture with different dominant factors emerges. The initial stage is dominated by flow rate, with temperature having no significant impact on fracture initiation and extension, resulting in a quick extension of around 100 meters in a matter of seconds. The second stage is temperature-dominated, where the isothermal cycle fracture size remains constant, but the fracture length and width gradually grow longer and wider with the increase in low-temperature cycle time, with the temperature significantly decreasing the lost flow rate threshold.

(3) Isothermal circulation results in a stable, elliptical lost fracture size, while the temperature-dominated stage in non-isothermal circulation generates a larger rectangular fracture profile.

In conclusion, temperature effects are similarly significant in procedures like hydraulic fracturing and must be considered when studying high-temperature and high-pressure formation lost circulation. The model, although ideal, clearly explains how temperature affects lost circulation, which differs significantly from the actual field conditions. A more accurate formation model is necessary to gain further insight into the impact of temperature on drilling fluid lost circulation.

REFERENCES

Alberty, M. W., & McLean, M. R. (2004). A physical model for stress cages. SPE annual technical conference and exhibition,

Chen, W., Wu, G., & Jia, S. (2010). The application of ABAQUS in tunnel and underground engineering. Beijing: Water Conservancy and Hydropower Press.

Feng, Y., Arlanoglu, C., Podnos, E., Becker, E., & Gray, K. (2015). Finite-element studies of hoop-stress enhancement for wellbore strengthening. SPE Drilling & Completion, 30(01), 38-51.

Feng, Y., & Gray, K. (2016). A parametric study for wellbore strengthening. Journal of Natural Gas Science and Engineering, 30, 350-363.

Feng, Y., & Gray, K. (2018). Modeling lost circulation through drilling-induced fractures. Spe Journal, 23(01), 205-223.

Feng, Y., & Gray, K. E. (2016). A fracture-mechanics-based model for wellbore strengthening applications. Journal of Natural Gas Science and Engineering, 29, 392-400.

Manual, A. U. (2020). Abaqus user manual. Abaqus.

Morita, N., & Fuh, G.-F. (2012). Parametric analysis of wellbore-strengthening methods from basic rock mechanics. SPE Drilling & Completion, 27(02), 315-327.

Peirce, A., & Detournay, E. (2008). An implicit level set method for modeling hydraulically driven fractures. Computer Methods in Applied Mechanics and Engineering, 197(33-40), 2858-2885.

Salehi, S. (2012). Numerical simulations of fracture propagation and sealing: Implications for wellbore strengthening. Missouri University of Science and Technology.

Shahri, M. P., Oar, T. T., Safari, R., Karimi, M., & Mutlu, U. (2015). Advanced semianalytical geomechanical model for wellbore-strengthening applications. Spe Journal, 20(06), 1276-1286.

van Oort, E., & Razavi, S. O. (2014). Wellbore strengthening and casing smear: the common underlying mechanism. IADC/SPE drilling conference and exhibition,

Wang, H. M., Soliman, M. Y., & Towler, B. F. (2009). Investigation of factors for strengthening a wellbore by propping fractures. SPE Drilling & Completion, 24(03), 441-451.

Wardeh, G., & Perrin, B. (2008). Freezing–thawing phenomena in fired clay materials and consequences on their durability. Construction and building materials, 22(5), 820-828.

Zhang, J., Alberty, M., & Blangy, J. (2016). A semi-analytical solution for estimating the fracture width in wellbore strengthening applications. SPE deepwater drilling and completions conference,